Research Square

Preprints are preliminary reports that have not undergone peer review.
They should not be considered conclusive, used to inform clinical practice,
or referenced by the media as validated information.

Ni single-atom catalyst boosts co-reactant free electrochemiluminescence for dual-signal detection and visual assay of I27L gene

Xiao-Hao Chen
Affiliated Hospital of Youjiang Medical University for Nationalities
Tao He
Affiliated Hospital of Youjiang Medical University for Nationalities
Jin-Xi Lu
Affiliated Hospital of Youjiang Medical University for Nationalities
Wang Li
Guangxi Huayin Medical Laboratory Co., Ltd
Zi-Ao Zong
Affiliated Hospital of Youjiang Medical University for Nationalities
Jing Wang
237054233@qq.com
Affiliated Hospital of Youjiang Medical University for Nationalities
Feng Guo
Affiliated Hospital of Youjiang Medical University for Nationalities
Guifen Jie
Qingdao University of Science and Technology

Research Article

Keywords: Ni SACs, ECL, mobile phone imaging, visualized Electrochemiluminescence System, Oxygen reduction reaction

Posted Date: November 23rd, 2026

DOI: https://doi.org/10.21203/rs.3.rs-11429682/v1

License: This work is licensed under a Creative Commons Attribution 4.0 International License.
Read Full License

Additional Declarations: No competing interests reported.

Ni single-atom catalyst boosts co-reactant free electrochemiluminescence for dual-signal detection and visual assay of I27L gene

Xiao-Hao Chen[a, b], Tao He[b, c], Jin-Xi Lu[b, c], Wang Li[d], Zi-Ao Zong[b, c], Jing Wang[b, c,*], Feng Guo[b, c,*], Guifen Jie[e*]

[a] *Center for Medical Laboratory Science, Affiliated Hospital of Youjiang Medical University for Nationalities, Guangxi, 533000, China*

[b] *Guangxi Key Laboratory of Artificial Intelligence for Genetic Diseases of Long-dwelling Nationalities, Baise, Guangxi, 533000, China*

[c] *Key Laboratory of Research on Environment and Population Health in Aluminium Mining Areas (Youjiang Medical University for Nationalities), Education Department of Guangxi Zhuang Autonomous Region, Baise 533000 Guangxi, China*

[d] *Guangxi Huayin Medical Laboratory Co., Ltd., Nanning 533000 Guangxi, China*

e *Key Laboratory of Optic-electric Sensing and Analytical Chemistry for Life Science, MOE; College of Chemistry and Molecular Engineering. Qingdao University of Science and Technology, Qingdao 266042, PR China*

ABSTRACT

Single-atom catalysts enhanced electrochemiluminescence (ECL) without co–reactants shows promising application potential for multiple sensing and imaging assay. This study utilizes a novel nickel single-atom catalyst (Ni SAC) with a unique electronic structure and excellent catalytic activity to significantly enhance the ECL of luminol without the need for exogenous co-reactants. Innovatively, a visualized dual-signal output ECL biosensor was developed for the detection of the I27L gene and smartphone-based imaging detection, opening new avenues for the application of single-atom catalysts. Ni SACs exhibit outstanding oxygen reduction reaction (ORR) activity, which could catalyze the reduction of dissolved oxygen (DO) to generate a

*Corresponding authors.

*E-mail address: 237054233@qq.com (J.W.); guofeng1510@yeah.net (F.G.) guifenjie@126.com.

large amount of reactive oxygen species (ROS). The ROS can oxidize luminol, producing a highly enhanced ECL signal while avoiding the toxicity and instability of the reactant H_2O_2. T In particular, the ECL signal is boosted to high enough for mobile phone imaging, which inspired us to introduce Ni SACs to the luminol ECL system for versatile biosensing and imaging assay of I27L gene. The target I27L gene first induces a multistage amplification process via DNA strand displacement technology, generating abundant DNA P. Subsequently, DNA P was used to attach plenty quenching probe PDANP@H2 to the Ni SACs/Au NPs/electrode. Based on the efficient ECL-RET effect between luminol and polydopamine (PDA) nanospheres, the intense ECL signal of the Ni SACs/luminol system is significantly quenched for dual-signal ECL detection and imaging of the target I27L gene. This work employs a novel Ni SACs-enhanced luminol ECL system technology and successfully applied to ECL analysis for biological fields and clinical disease diagnosis.

Keywords Ni SACs, ECL, mobile phone imaging, visualized Electrochemiluminescence System, Oxygen reduction reaction

Introduction

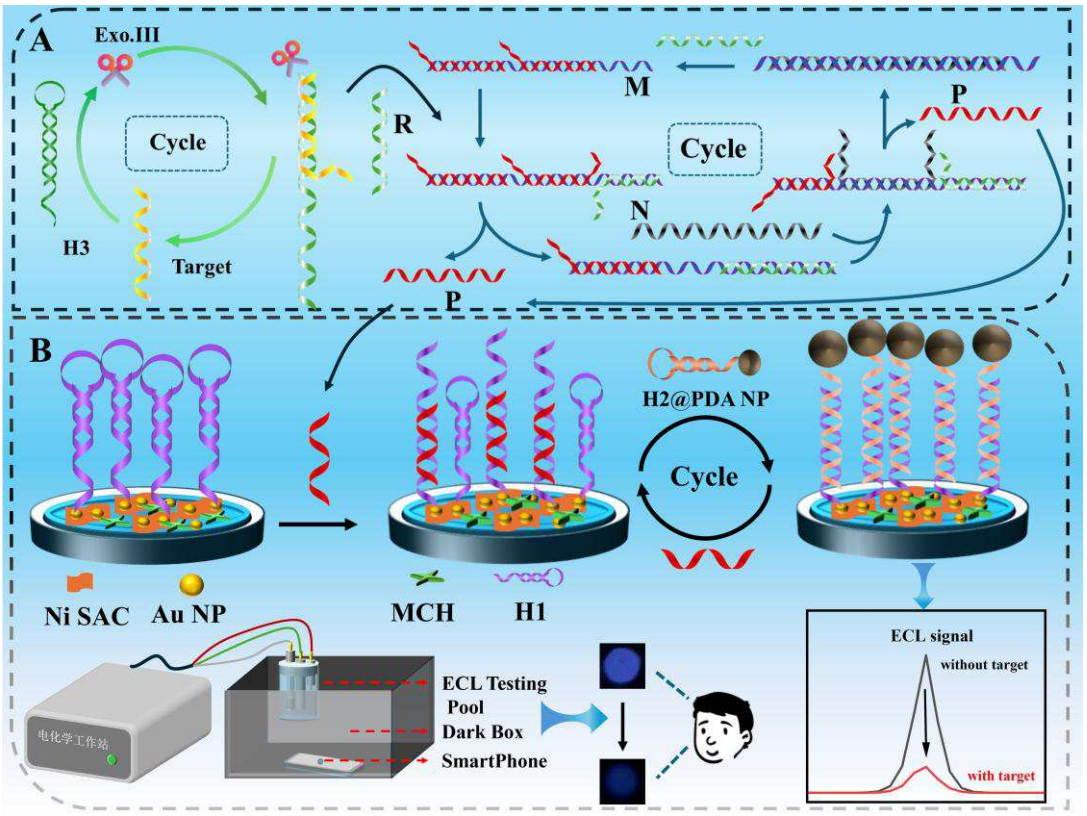
Most diabetes cases are the interaction results of gene and environmental factors, they can be roughly divided into two categories, both of which are polygenic. However, with increase of type 2 diabetes among young adults, accurate classification is of great clinical significance, which may determine the choice of treatment plan and ultimately affect the long–term life quality of patients [1]. Maturity‐onset diabetes of the young (MODY) is a rare subtype accounting for about 1% of all cases. At present, 14 MODY genes have been identified, most cases are derived from hepatocyte nuclear factor 1α (HNF1A) mutation [2], and I27L gene variant is closely related to the sensitivity of a single gene to diabetes [3]. In addition, it has been determined that the I27L gene is more likely to be a resistant marker to HNF1A–MODY mutation [4]. Therefore, the development of a new I27L detection strategy with high sensitivity and specificity should be the focus of the early monitoring and diagnosis of HNF1A‐MODY [5].

Electrochemiluminescence (ECL) has the advantages of high sensitivity, easy operation and low reagent consumption, and has been widely used in environmental monitoring [6,7], drug safety [8], clinical diagnosis [9], biological imaging [10,11] and food safety [12] and other fields. As a highly promising anode ECL material, Luminol has attracted wide attention for high luminous efficiency, non–toxicity and low oxidation potential. Although the typical co–reactant H_2O_2 induces significant ECL signals, the self–degradation and biotoxicity of H_2O_2 lead to the difficulty for wide application. For some other ECL systems based on Luminol, MOFs [13] and 3D porous g–C_3N_4[14], dissolved oxygen is an essential co–reactant [15-17]. In the traditional ECL system, reactive oxygen species generated by dissolved oxygen through ORR process participates in ECL reaction. Due to the inherent kinetic limitations of ORR process that lead to the low efficiency of ROS generation, exploring high–efficiency co–reaction accelerator to promote the mass production of ROS has become an important research direction in this field. [18]. For ECL systems with high luminous efficiency, mobile phone imaging has become a commonly used method, which has many advantages such as simple, fast, intuitive and real–time detection [19,20].

Dissolved oxygen (DO) as an endogenous co–reactant [21], with the characteristics of non–toxic and stable, is considered a potential substitute for H_2O_2 in ECL system. Active intermediates such as $HO^{\bullet}$, $^1O_2$, and $O_2^{\bullet-}$ exhibit similar catalytic performance to H_2O_2 in ECL systems, suggesting their potential as alternative reactive species [22]. Converting DO into ROS requires the participation of another co-reaction accelerator (CRA), such as high–entropy oxides [23], iron monoatomic catalyst (Fe SAC) [24], nanocrystalline [25], polyvalent manganese oxide micro flower [26] and others, which are used to improve the ECL performance. It is still challenging and promising to explore new catalysts for ultra–sensitive ECL sensing.

The single–atom catalyst shows significant application prospects for biomarker detection, environmental pollution monitoring and other fields. [27]. Compared with traditional nanoscale catalysts, SAC's clearly defined catalytic sites make it easier to study the ECL process from an experimental and theoretical perspective [28]. SACs

display excellent catalytic performance and have made great breakthroughs in the fields of electrocatalysis, photocatalysis and ECL [29]. In addition, the extremely strong catalytic ability of SAC can change the microenvironment of reaction interface to regulate the catalytic site, providing a platform for studying the transformation and reaction mechanism during ECL process [30].



Scheme 1. Schematic diagram of the dual-signal output electrochemiluminescence biosensor based on Ni single‐atom catalyst and target amplicication for detection and imaging assay of gene I27L.

Based on the excellent catalytic performance of SACs and nucleic acid cycling amplification technique, this work innovatively applies Ni SAC to multifunctional ECL sensing and imaging detection. Thanks to the strong ORR catalytic ability of Ni SAC, highly intense ECL emission of Luminol was achieved with no need of co–reactants, which can be used to dual output of ECL signal and imaging value. Scheme 1A is the target magnification process. Firstly, target I27L and hairpin H3 hybridize to form a double–stranded DNA complex. After Exo III. initiates amplification reaction, a large number of single–stranded DNA R. Triggers are produced. Then R and M

perform DNA strand displacement reaction, and initiate a cyclic amplification reaction with the participation of DNA N, outputting many DNA strands P. Scheme 1B are the construction and imaging process of the dual-signal output ECL biosensor. P strand firstly opens H1 on the electrode, then introduces the quenching probe PDANP@H2 via DNA cycling hybridization, realizing obvious change of ECL signal and mobile phone imaging intensity for gene assay. Therefore, the designed sensing system introduces Ni SACs to achieve highly sensitive ECL detection and high‐resolution imaging analysis, which has great application prospects in biological analysis and clinical disease diagnosis.

Experimental

Reagents and Apparatus, Synthesis of Au NPs, Polyacrylamide gel electrophoresis analysis, were shown in the Supporting Information.

Preparation of Ni SACs

Ni SAC was synthesized based on previous research [31,32]. Nickel tetrahydrated acetate (12.4 mg) and 1,10-phthalophyrin monohydrate (29.7 mg) were added to 2 mL of ethanol, and stirred for 10 minutes. Then carbon black (69.6 mg) was dissolved in the mixture, heated in an oil bath to 60 ℃ and kept continuous reaction for 4 hours. The product was placed at 80 ℃ to dry overnight, put the ground product in a ceramic crucible, and heated in a 600 ℃ nitrogen atmosphere at a speed of 10 ℃/min in a tube furnace for 2 hours. After that, the product is cooled to room temperature and ground in an agate mill. Then, the powder was etched in 2 M H_2SO_4 at 80 ℃ for 48 hours. The final product (named Ni SACs here) was dried at 80 ℃ overnight.

Synthesis of PDA NPs

Polydopamine nanoparticles were prepared according to the work [33,34]. 3 mL of ammonia solution, 90 mL of deionised water and 40 mL of anhydrous ethanol was mixed at 30 ℃, and lightly stirred for 0.5 h. Then, 0.5 g of dopamine hydrochloride was dissolved in 10 mL of deionised water, and then poured into the above-mentioned mixed solution. The color of the solution immediately turned light yellow and

gradually turned dark brown. After continuous stirring for 12 hours, the product was washed 3 times to obtain PNANPs.

Preparation of H2-PDA NPs probe

100 μL of 0.1 M EDC and 25 μL of 0.1 M NHS solution were added to 100 μL of 1 μM H2 solution, and activated at 37 ℃ for 1 h. Then 25 μL of 0.05 mg/mL PDA NPs was added, and incubated at 37 ℃ for 2 h, centrifuged and dispersed in 125 μL.

Cyclic amplification process

Firstly, H2 stock solution was annealed at 95 °C and then cooled to room temperature at a rate of 6 °C/min. 50 μL 1 μM hairpin H3 was incubated with target DNA of different concentrations for 1.5 hours, then 10 U of Exo was III added, incubated in a 37 ℃ shaker for 15 minutes. Finally, the reaction system is heated to 75 ℃ for 15 minutes to terminate the reaction, thus the product DNA Trigger R was obtained.

Secondly, 5 μL 10 μM DNA M strands and 10 μL 10 μM DNA P strands were mixed, annealed at 95 ℃ and cooled to room temperature to form a three stranded DNA complex. Then 30 μL of the above mentioned shearing product was mixed with 10 μL 10 μM of DNA N strand and the three strand complex, and incubated in a 37 ℃ shaker for 2 hours. Ultimately, we obtained more than twice the targeted amount of cyclic probe P.

Construction of the ECL biosensor for detecting I27L gene

6 μL of 2 mg/mL Ni SACs solution (deionized water: ethanol: nafion = 20:79:1) was dropped on the GCE electrode and naturally dried. After 4 μL of Au NPs solution was added and dried, 6 μL 1 μM of hairpin H1 activated by EDC and NHS was added and incubated at 4 ℃ for 12 hours. Then 1 mM MCH was added for 1.5 hours, and 5 μL of the amplification product P was dropped to the electrode and reacted for 1.5 hours. Finally, 5 μL of PDANP@H2 solution was added and incubated for 1.5 hours, then rinsed with deionized water.

Related measurement parameters of the dual-signal output biosensor

ECL sensor measurement parameters: Using the three-electrode system. GCE as the working electrode, platinum wire as the counter electrode and Ag/AgCl electrode

as the reference electrode. ECL detection is carried out on BR buffer (0.1 M, pH=10) containing 2 mM Luminol. The scanning potential, scanning rate and photomultiplier are -0.4−0.4 V, 0.2 V/s, and 400V respectively.

The mobile phone ECL imaging parameters: Using a three-electrode system, which is the same as the ECL sensor measurement. And the electrolyte solution did not change. The scanning voltage was set −0.4~0.4 V. The scanning rate was 0.2 V/s. Significantly, the ECL imaging process is carried out in the dark box with a mobile phone (iPhone 14 Pro Max).

Results and discussion

Optimization of experimental conditions were shown in the Supporting Information.

Characterization of Ni SACs and PDA NPs

Fig. 1A, B show the scanning electron microscope (SEM) and transmission electron microscope (TEM) images of Ni SAC respectively, the average diameter of Ni SAC is about 20-30 nm, and no metal-nickel nanoclusters or nanoparticles are found on the carbon black substrate. In addition, disordered lattice stripes consistent with carbon black were also found in the HRTEM image, which also proved that metallic nickel nanoparticles do not exist (Fig. 1C). In order to further characterize the dispersion state of Ni atoms in Ni SAC, the HAADFSTEM test was carried out. In Fig. 1D, many bright dots are detected on the carbon-black substrate, which means that Ni exists in atomic form. Fig. 1E is TEM of Au NPs, the spherical particle size is about 20 nm. Fig. 1F is the SEM characterization of PDA NPs, showing the regular spherical structure of PDA NPs, and the average length is about 70-160 nm.

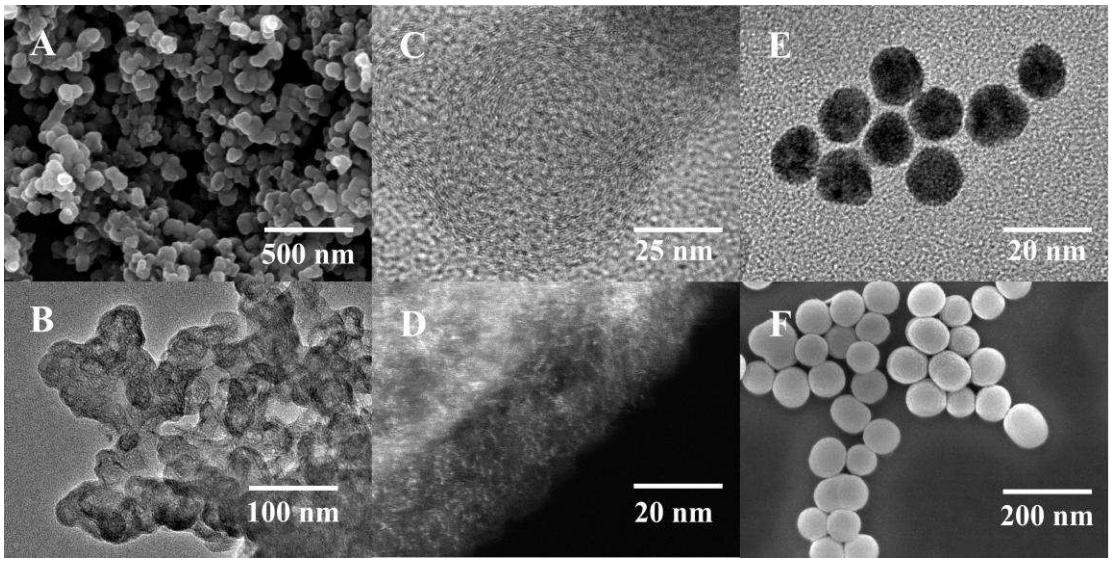


Fig. 1. (A) SEM image of Ni SAC, (B) TEM image of Ni SAC, (C) HRTEM image of Ni SAC, (D)HADDF-STEM image of Ni SACs, (E) TEM image of Au NPs, (F) SEM image of PDA NPs.

In order to study the elements in Ni SAC, the XPS spectrum of Ni SAC is analyzed. Fig. 2A shows the presence of Ni, C, N and O, and O may be caused by the oxidation of C and N. In addition, the C1s high-resolution spectra contains four characteristic peaks, corresponding to the following chemical bond states: C-N at 284.8 eV, C-C at 283.97 eV, C-O at 286.04 eV, and O=C–O at 290.6 eV (Fig. 2B). N1s high-resolution XPS spectrum also displays four characteristic peaks, corresponding to graphite N (401.5 eV), pyrrole N (400.9 eV), pyridine N (398.5 eV) and Ni-N (400.09 eV) (Fig. 2C). The peak values of 872.4 eV and 855.1 eV belong to Ni $2p_{1/2}$ and Ni $2p_{3/2}$ respectively (Fig. 2D). In Fig. 2F, XRD spectrum of Ni SAC is highly consistent with the N-C, showing only the (002) and (100) crystal surface characteristic peaks of graphite, and no diffraction signals from any Ni nanoparticles or crystals were observed, indicating that Ni exists in atomic-scale dispersion.

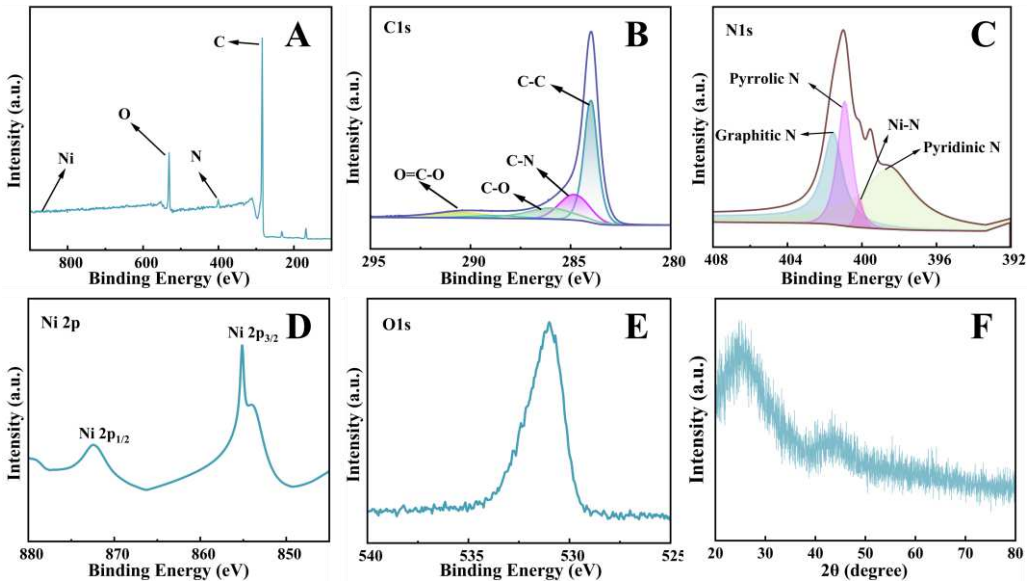


Fig. 2. (A) XPS spectrogram of Ni SAC, (B) C, (C) N, (D)Ni 2p, (E)O, (F) XRD characteristic spectrum of Ni SAC.

The DNA cycling-cleavage and amplifiction process was verified by polyacrylamide gel electrophoresis (PAGE) (Fig. S1).

Characterization of PDANP–H2 probe

In Fig. S2, the PDA NPs–H2 probe was characterized using UV-vis absorption spectra. It can be seen that the hairpin H2 has obvious characteristic absorption at a wavelength of 260 nm, and the synthesized PDA NPs has a broad absorption spectrum under the entire ultraviolet wavelength. After the two are assembled, the complex produces an obvious characteristic at 260 nm. The absorption peak proved that PNANP–H2 was successfully assembled.

Feasibility of the dual-signal output ECL biosensor for detecting I27L gene

UV−vis of PDA NPs and ECL emission spectrum of luminol indicated the RET between PDA NPs and luminol. The ECL emission spectra of luminol had a maximum emission wavelength of 425 nm (Fig. 3A, orange curve). UV−vis of PDA NPs (blue curve) had a broad absorption at 200−700 nm with a good spectral overlap with the emission of luminol. In Fig. 3B, the modified electrodes were studied by electron transfer resistance (Ret) of $[Fe(CN)_6]^{3-/4-}$. Due to the good conductivity of Ni SACs, the Ret of SACs on GCE significantly reduced (curve a) compared with that of

the bare electrode (curve b).

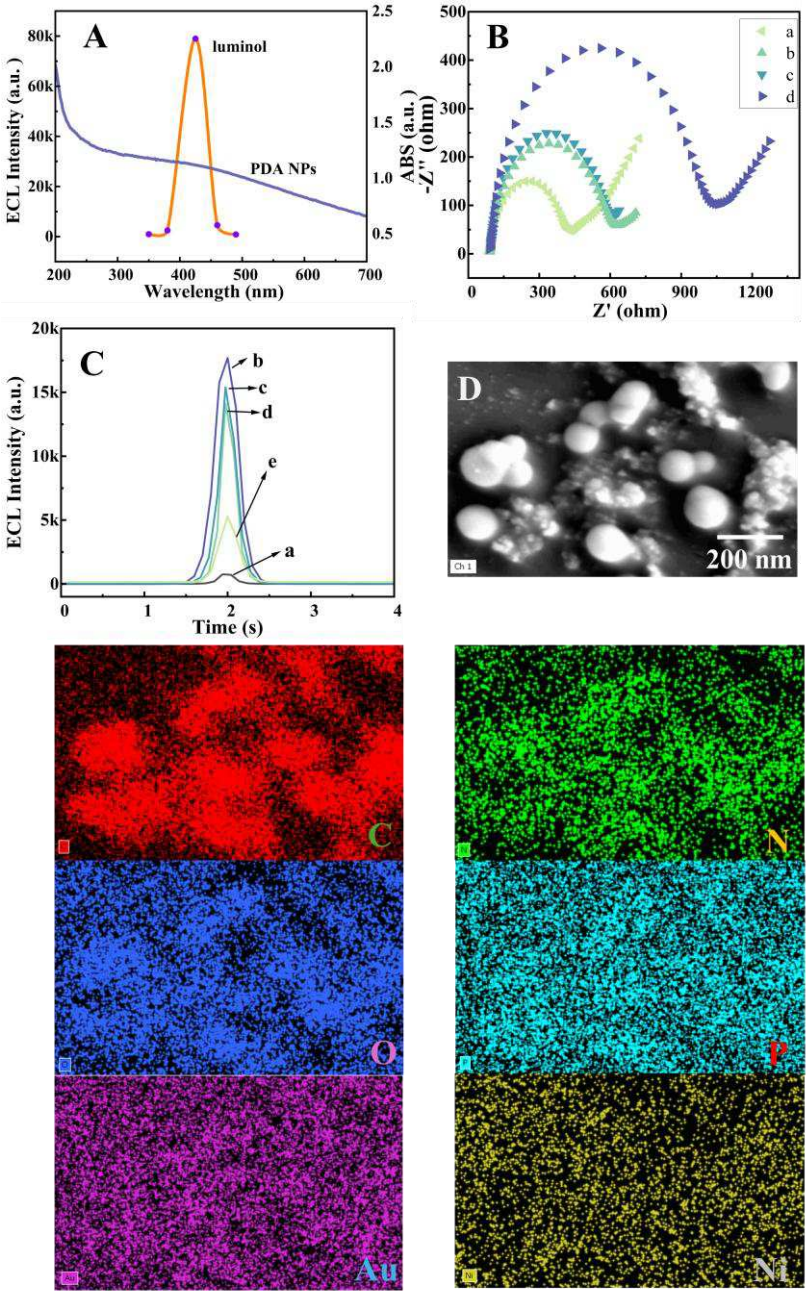


Fig. 3. (A) UV−vis absorption spectrum of PDA NPs and ECL spectrum of luminol: (a) PDA NPs/H2, (b) PDANPs, (c) H2; (B) Electrochemical impedance (EIS) of the electrode at different stages: (a) Ni SACs/Au NPs/GCE, (b) bare GCE, (c) Ni SACs/Au NPs/H1/P/GCE, (d) Ni SACs/Au NPs/H1/H2 -PDANPs/GCE; (C) ECL intensity of (a) Bare GCE, (b) Ni SAC/Au NPs, (c) Ni SAC/Au NPs/H1, (d) Ni SAC/Au NPs/H1/H2-PDANPs, (e) Ni SAC/Au NPs /H1/P/H2/PDA NP; (D) SEM and the corresponding element mapping images of Ni SAC/Au NP/H1/H2-PDA NPs.

When H1 and DNA P were introduced, the impedance increased (curve c). When H2-PDANPs as quenching probe hybridized with H1 on the electrode, the impedance significantly increased (curve d).

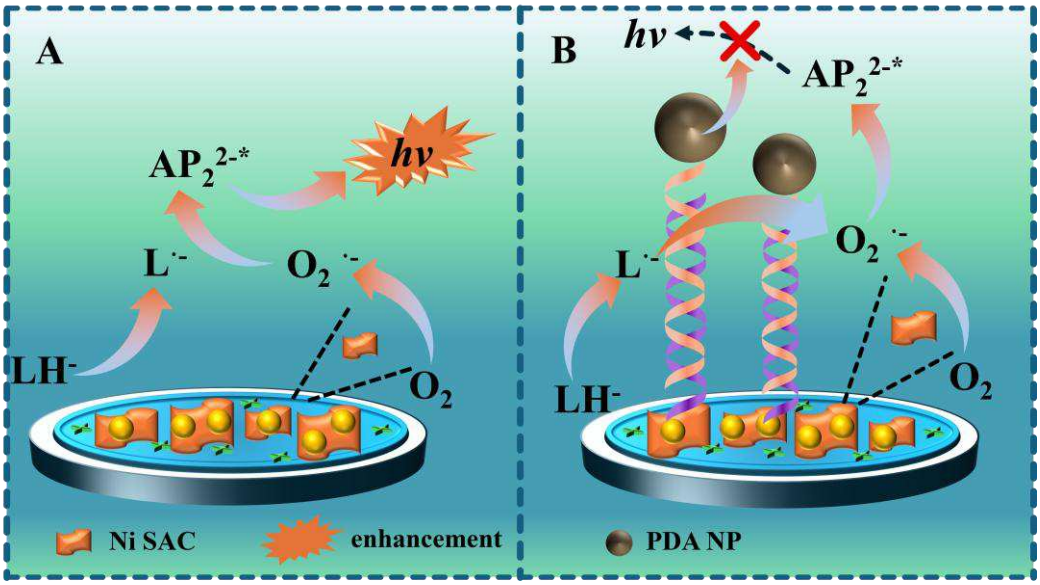
Moreover, the fabrication of ECL biosensor was proved by ECL signals at each stage. In Fig. 3C, curve a is the signal of the bare electrode. Curve b is an obviously strong ECL signal after modifying Ni SACs and Au NPs on GCE, suggesting that the excellent catalytic activity of Ni SACs highly boost ECL of luminol. After connecting hairpin H1 to the electrode, ECL signal is slightly reduced (curve c), which may be due to the increase in electrode surface impedance. When the electrode is further directly incubated with the PDANP-H2 probe, the signal only slightly drops (curve d), indicating that H2 cannot be connected to H1 in the absence of target. After the target-amplification product P chain and PDANP-H2 were further present, H1 is opened and hybridised with H2, the energy resonance transfer effect of PDANPs and Luminol results in signal extinction (curve e), realizing detection of target I27L gene. The above results proved the feasibility of the designed biosensor.

Finally and importantly, the biosensor assembly is proved through SEM and EDS. After the PDA NPs probe was connected to the Ni SACs-modified electrode via target-amplification product, both Ni SACs and PDA NPs were observed (Fig. S2). In addition, all elements (C, N, O, P, Au and Ni) distribution from Ni SAC/PDA NP complex were proved by EDS mapping and energy spectrum images (Fig. 3D), suggesting construction of the ECL biosensor.

Mechanism of the Ni SAC/Luminol System

Currently, there are very few experimental studies related to ECL using Ni NPs (Nanoparticle). Here, we selected Ni NPs for performance testing to investigate the performance differences between them and Ni SACs. The study investigated the impact of Ni SAC (Single Atom Catalyst) and Ni NPs active sites on the ECL (Electrochemiluminescence) performance of the luminol-dissolved O_2 system. As shown in Fig. S3A, the use of Ni NPs as co-reactant accelerators resulted in only weak ECL emission. However, upon introducing Ni SAC as a co-reactant promoter, the ECL intensity was significantly enhanced, indicating the great potential of Ni SAC

in promoting the ECL reaction between luminol and dissolved O_2. UV−vis of PDA NPs and ECL emission spectrum of luminol indicated the RET between PDA NPs and luminol. The ECL emission spectra of luminol had a maximum emission wavelength of 425 nm (Fig. S3B, orange curve). UV−vis of PDA NPs (blue curve) had a broad absorption at 200−700 nm with a good spectral overlap with the emission of luminol. Based on previous research [35,36] combined with the experimental and computational results with 1 pM I27L target. A certain amount of different concentrations of benzoquinone (BQ), tert-butyl alcohol (t-BA), and ascorbic acid (AA) were used to remove $O_2^{\bullet-}$, $OH^{\bullet}$, and total ROS, respectively. According to the data in Figure S3C, 5 mM BQ and AA had a significant impact on the catalysis of SAC, almost quenching the ECL emission, indicating that $O_2^{\bullet-}$ plays a crucial role in the ECL reaction. In contrast, a decrease in the ECL signal was observed in the t-BA experiment, suggesting the presence of $OH^{\bullet}$ in the ECL process. Unlike Ni SAC, in the case of Ni NPs, the signal decreased upon the addition of BQ, indicating that $O_2^{\bullet-}$ also participates in the reaction but with weaker intensity. However, in the experiments with t-BA and AA, the signal remained almost unchanged. These experiments briefly demonstrate that the performance of Ni SAC is significantly superior to that of Ni NPs, and it is recommended to use Ni SAC as a co-reactant promoter in the luminol/dissolved O_2 ECL system. The ECL mechanism is shown in Scheme 2A and following equations. During cathodic scanning, the process begins with the adsorption of dissolved O_2 at the Ni SACs interface. Subsequently, the SACs active site catalyzes the reduction of O_2 to produce more superoxide radical ($O_2^{\bullet-}$). The electrochemical oxidation of luminol anions (LH^-) produces numerous luminol anion radicals ($L^{\bullet-}$). Then, abundant $O_2^{\bullet-}$ and $L^{\bullet-}$ can react in situ on the Ni SACs surface to generate more excited-state intermediate (3-amino-phthalate radical anion, AP_2^{2-*}), generating a significantly enhanced ECL emission [32]. As can be seen from Scheme 2B, when the PDA NP quenching probe is introduced through target, due to its UV−vis had a broad absorption at 200−700 nm with a good spectral overlap with the emission of luminol., the ECL signal is quenched.



Scheme 2. The possible mechanisms of (A) Ni SACs boost ECL of Luminol/ DO system; (B) ECL quenching of Luminol by PDA NPs probe.

$$O_2 + e^- \rightarrow O_2^{\bullet -} \quad (1)$$

$$LH^- - e^- \rightarrow L^{\bullet -} + H^+ \quad (2)$$

$$L^{\bullet -} + O_2^{\bullet -} \rightarrow LO_2^{2-} \quad (3)$$

$$LO_2^{2-} \rightarrow AP_2^{2-*} + N_2 \quad (4)$$

$$AP_2^{2-*} \rightarrow AP_2^{2-} + h\nu \quad (5)$$

Dual-mode sensing and imaging ECL platform for detecting I27L gene

In Fig. 4A, when the concentration of I27L gene increases from 1 fM to 10 nM, the ECL signals gradually decreases. As the increasing I27L gene induces to generate more DNA Triggers, then the generated DNA P increases. Finally, more PDA NPs quenching probes can be connected to the electrode via DNA P, leading to decreased ECL. The change of ECL displays good linear relation with I27L gene in the range of 1 fM-10 nM (Fig. 4B). The linear equation is: $y=1883.98 \log x + 12554.92$ $R^2=0.981$, and its LOD is 0.606 fM. Moreover, the biosensor can simply present intuitive mobile phone ECL imaging results to target. In Fig. 4C, as the concentration of I27L gradually increases, the blue imaging brightness gradually decreases. In Fig. 4D, the change of RGB value shows linear with the concentration of I27L gene from 1 fM to 1 nM, LOD is 0.063 fM.

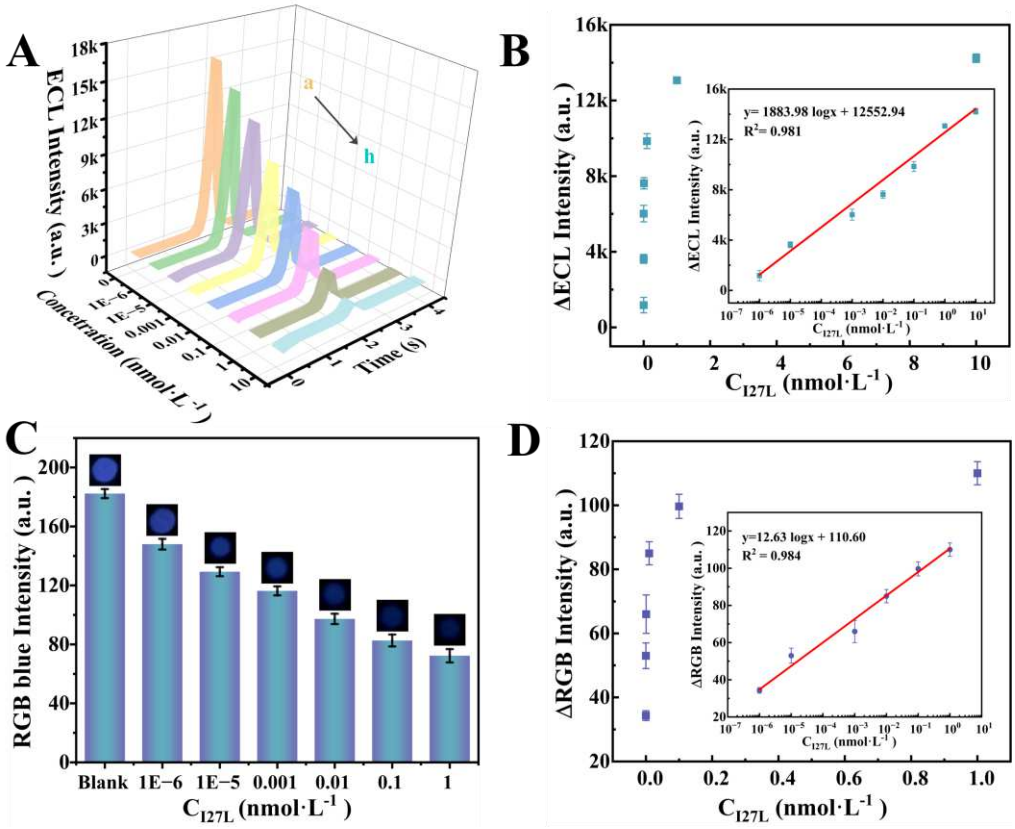


Fig. 4. (A) ECL signals with different concentrations of I27L gene (a–h: 0, 1 fM–10 nM); (B) ECL calibration plot for I27L gene detection; (C) RGB value intensity with different concentrations of I27L gene (0, 1 fM–1 nM); (D) RGB calibration plot for I27L gene detection.

Application of this dual-signal output biosensor (Table S2 and Table S3)

To evaluate the applicability of the biosensor, we performed recovery tests using I27L-spiked human serum samples at varying dilution factors, following standard analytical protocols. First, the human serum was diluted 10-fold with 0.01 M PBS buffer (pH 7.4) and used as the target for constructing the ECL biosensor. Subsequent experiments were performed in the same manner as before. As shown in Table S2, the recovery rate is between 98.81% and 102.17%, and the RSD is between 5.51% and 7.01%. This proves the potential of the DNA biosensor in the analysis of sample serums (Supporting Information Table S2). Compared with other DNA sensors, our multi-mode co-reactant-free ECL sensor shows a wider dynamic range and a lower LOD for target DNA analysis (Supporting Information Table S3).

Conclusions

This study utilizes Ni SAC to significantly enhance the ECL of luminol without the need for exogenous coreactants. The high-intensity ECL signal enables detection via smartphone imaging. Consequently, a dual-signal output ECL biosensor was successfully developed based on this nickel single-atom/luminol ECL system. It has been applied for highly sensitive and accurate ECL detection and imaging of diabetic markers. Firstly, Ni SACs display very high catalytic efficiency, thus Luminol ECL signal is more prominent and no co-reactants are required, which guaranted convenient trace ECL detection and imaging assay of targets. Moreover, we ingeniously designed a triple magnification mode, which greatly increased the quantity of target magnification products and much enhanced the detection sensitivity. Importantly, the dual-mode output can meet the test needs of different conditions, and can carry out fast and intuitive color comparison detection. In addition, by replacing the hairpin probe H3, it can be used for the detection of other genes, demonstrating the versatility of the sensor. The ECL sensor provides an accurate and intuitive detection method for MODY's genetic detection, which may provide suitable applications in clinical testing.

Acknowledgements

This work was supported by the Fundamental Research Funds for the Guangxi Natural Science Foundation Program (No. 2025GXNSFHA069268) and the Open Competition Project of Guangxi Plateau Discipline (2026), Youjiang Medical University for Nationalities (YY2026GYY29).

Research funding

This research did not receive funding.

Declaration of Artificial Intelligence (AI) in preparation of the manuscript and figures

AI: Not Applicable.

References

1 Amed S, Oram R (2016) Maturity-Onset Diabetes of the Young (MODY): Making

the Right Diagnosis to Optimize Treatment. Can. J. Diabetes. 40:449–454.

2 Anik A, Çatli G, Abaci A, Böber E (2015) Maturity-onset diabetes of the young (MODY): an update. J Pediatr Endocr Met. 28:251–263.

3 Xue H, Zeng L, Liu S (2023) Unraveling the link: exploring the causal relationshipbetween diabetes, multiple sclerosis, migraine, and Alzheimer's disease through Mendelian randomization. Front Neurosci. 17:1233601.

4 Peixoto. Barbosa R, Peixoto A F, Giuffrida F M A (2020) Update on clinical screening of maturity-onset diabetes of the young (MODY). Diabetol Metab Syndr. 12:50.

5 Zhang Y, Cao X, Wang Z R. , Cheng Z J, Zhong Y, Zhang Z, Liu A L, Lei Y (2025) Enhanced bipolar electrode electrochemiluminescence biosensor for ultrasensitive monitoring of alkaline phosphatase activity during osteoblast differentiation by integrating electrocatalytic and enzymatic strategies. Sensors & Actuators: B. Chemical. 423:136823.

6 Du F, You N, Hu X P, Xu F L, Liu G (2026) Smartphone-Based Electrochemiluminescence Sensors. NENP. 2:16.

7 Zhou Y, Wu Y, Luo Z, Ling L, Xi M Z, Li J H, Hu L Y, Wang L, Gu W L, Zhu C Z (2024) Regulating Reactive Oxygen Species over M–N–C Single-Atom Catalysts for Potential-Resolved Electrochemiluminescence. J. Am. Chem. Soc. 146:12197–12205.

8 Jiang Q Q, Li Y J, Wu Q, Wang X, Luo Q X, Mao X L, Cai Y J, Liu X, Liang R P, Qiu J D (2023) Guest Molecular Assembly Strategy in Covalent Organic Frameworks for Electrochemiluminescence Sensing of Uranyl. Anal. Chem. 95:8696–8705.

9 Huang C C, Wang Y H, Fu B H, Guan Y Y, Jie G F (2025) High-performance Zr-MOFs electrochemiluminescence biosensor and amplification technology for study of circulating amplification factor and detection of BRCA-1. Microchem. J. 219:115972.

10 Ge J J, Li R Q, Wei Y P, Mao C J, Zhu H (2026) Nanocluster Luminophores for Electrogenerated Chemiluminescence Imaging. NENP. 2:20.

11 Lu Y W, Huang X D, Wang S R, Li B X, Liu B H (2023) Nanoconfinement–Enhanced Electrochemiluminescence for in Situ Imaging of Single Biomolecules.

ACS Nano. 17:3809–3817.

12 Yu S Q, Hu X F, Pan J B, Lei J P, Ju H X (2023) Nanoconfined Cathodic Electrochemiluminescence for Self-Sensitized Bioimaging of Membrane Protein. Anal. Chem. 95:16593–16599.

13 Wang C Y, Zhang Y T, Liu S S, Yin Y S, Fan G C, Shen Y Z, Han H Y, Wang W J (2023) Allosteric probe-triggered isothermal amplification to activate CRISPR/Cas12a for sensitive electrochemiluminescence detection of Salmonella. Food Chem. 425:136382.

14 Lai D X, Mu Z D, Zuo J L, Zhou J X, Zhang Q F, Chen K Y, Bai L J, Liang H W (2023) Perylene-Based Electrochemiluminescent Metal–Organic Frameworks for Detection of Zearalenone. ACS Appl. Nano Mater. 6:22416–22425.

15 Li R F, Jing Z W, Yang G M, Yuan R, Hu F X, Chen S H (2023) Nickel Single–Atom Catalyst Boosts Electrochemiluminescence of Graphitic Carbon Nitride for Sensitive Detection of HBV DNA. Anal. Chem. 95:18207–18214.

16 Wu B X, Dong Y P (2025) Dual-potential ECL system based on cucurbit 6 uril enhanced anodic luminol emission and cathodic g-C_3N_4 emission and its sensing application for glucose. J. Electroanal. Chem. 979:118916.

17 Liu M R, Wei J L, Lin S J, Cai Z X (2024) Triggering Anodic Luminol Electrochemiluminescence through Electrostatic Interactions: An Innovative Approach Utilizing Conductive Metal-Organic Framework Co–HHTP. ACS Appl. Electron. Mater. 6:2375–2382.

18 Liu H T, Jiang F, Dong H, Li Y Y, Liu Q, Wang S J, Li Y Y, Wei Q (2024) Highly efficient electrochemiluminescence based on Lu@Ov–ZMO as an ECL emitter for ultrasensitive detection of CA242. Microchem. J. 200:110482.

19 Zhong W, Fu Y Z, Chen X Q, Lu C (2024) Understanding Reactive Oxygen Species in Potential-Resolved Electrochemiluminescence of Luminol-Dissolved O_2. J. Phys. Chem. C. 128:13155–13161.

20 Lin Z J, Chen X M, Jia T T, Wang X D, Xie Z X, Oyama M, Chen X (2009) Fabrication of a Colorimetric Electrochemiluminescence Sensor. Anal. Chem. 81:830–833.

21 Cai Q Q, Li H K, Li Z K, Jie G F (2024) Study on the Electrochemiluminescence Emission Mechanism of HOF-14 and Its Multimode Sensing and Imaging Application. Anal. Chem. 96:16900–16909.

22 Wang L, Jiang H, Zhang J, He X H, Li F F, Feng J, Pan B (2024) Identifying the photoproduction sites of reactive oxygen species in dissolved black carbon: A remarkable role of oxygenated functional groups. Appl. Catal. B Environ. 351:123921.

23 Li J W, Yang J, Zhu L, Liu Y J, He Y C, Li Y C (2024) Ultrastable Luminol–OH^-–(Ni–WOx–CNT) ECL System with High Strength and Its Applications in Sensing. Anal. Chem. 96:9953–9960.

24 Bushira F A, Wang P, Jin Y D (2022) High-Entropy Oxide for Highly Efficient Luminol–Dissolved Oxygen Electrochemiluminescence and Biosensing Applications. Anal. Chem. 94:2958–2965.

25 Bushira F A, Kitte S A, Xu C, Li H J, Zheng L R, Wang P, Jin Y D (2021) Two-Dimensional-Plasmon–Boosted Iron Single-Atom Electrochemiluminescence for the Ultrasensitive Detection of Dopamine. Hemin, and Mercury, Anal. Chem. 93:9949–9957.

26 Liao H X, Jin C H, Zhou Y, Chai Y Q, Yuan R (2019) Novel ABEI/Dissolved O_2/Ag_3BiO_3 Nanocrystals ECL Ternary System with High Luminous Efficiency for Ultrasensitive Determination of MicroRNA. Anal. Chem. 91:11447–11454.

27 Yang R, Liu J L, Chai Y Q, Yuan R (2020) MnOx MFs as a coreaction accelerator for the construction of a novel ternary electrochemiluminescence system: ultrasensitive detection of microRNA. Chem. Comm. 56:976–979.

28 Ji S F, Chen Y J, Wang X L, Zhang Z D, Wang D S, Li Y (2020) Chemical Synthesis of Single Atomic Site Catalysts. Chem. Rev. 120:11955.

29 Wang Y, Tang Y J, Zhou K (2019) Self-Adjusting Activity Induced by Intrinsic Reaction Intermediate in Fe–N–C Single-Atom Catalyst. J. Am. Chem. Soc. 141:14119.

30 Yang H B, Hung S F, Liu S, Yuan K D, Miao S, Zhang L P, Huang X, Wang H Y, Cai W Z, Chen R, Gao J J, Yang X F, Chen W, Huang Y Q, Chen H M, Li C M, Zhang

T, Liu B (2018) Atomically dispersed Ni as the active site for electrochemical CO_2 reduction. Nat. Energy. 3:140–147.

31 Luo X, Wei X Q, Wang H J, Gu W L, Kaneko T, Yoshida Y, Zhao X, Zhu C Z (2020) Secondary-Atom–Doping Enables Robust Fe–N–C Single–Atom Catalysts with Enhanced Oxygen Reduction Reaction. Nano−Micro Lett. 12:163.

32 Gu W L, Wang X S, Wen J, Cao S Y, Jiao L, Wu Y, Wei X Q, Zheng L R, Hu L Y, Zhang L Z, Zhu C Z (2021) Modulating Oxygen Reduction Behaviors on Nickel Single-Atom Catalysts to Probe the Electrochemiluminescence Mechanism at the Atomic Level. Anal. Chem. 93:8663–8670.

33 Liu J, Kang L, Smith S, Wang C (2021) Transmembrane MUC18 Targeted Polydopamine Nanoparticles and a Mild Photothermal Effect Synergistically Disrupt Actin Cytoskeleton and Migration of Cancer Cells. Nano Lett. 21:9609–9618.

34 Liu Y L, Ai K L, Liu J H, Deng M, He Y Y, Lu L H (2012) Dopamine–Melanin Colloidal Nanospheres: An Efficient Near–Infrared Photothermal Therapeutic Agent for In Vivo Cancer Therapy. Adv. Mater. 25:1353–1359.

35 Ma Y C, Zhang Y, Gao J Q, Ouyang H, He Y, Fu Z F (2022) PEGylated Ni Single-Atom Catalysts as Ultrasensitive Electrochemiluminescent Probes with Favorable Aqueous Dispersibility for Assaying Drug–Resistant Pathogens. Anal. Chem. 94:14047–14053.

36 Xi M Z, Wu Z C, Luo Z, Ling L, Xu W Q, Xiao R S, Wang H J, Fang Q, Hu L Y, Gu W L, Zhu C Z (2023) Water Activation for Boosting Electrochemiluminescence. Angew. Chem. Int. Ed. 62: e202302166.

Supplementary Files

This is a list of supplementary files associated with this preprint. Click to download.

- MA10.19S.docx